Slope error correction on X-ray reflection gratings by a variation of the local line density

ADAM KUBEC,[1,2,*] NAZANIN SAMADI,[1] MANUEL LANGER,[1,3] FLORIAN DÖRING,[1] BENEDIKT RÖSNER,[1] VITALIY A. GUZENKO,[1] NAZARET ORTIZ HERNÁNDEZ,[1,4] URS STAUB,[1] ROLF FOLLATH,[1] JÖRG RAABE,[1] AND CHRISTIAN DAVID[1]

[1]*Paul Scherrer Institut, Forschungsstr. 111, CH-5232 Villigen-PSI, Switzerland*
[2]*Current address: XRnanotech GmbH, Forschungsstr. 111, CH-5232 Villigen-PSI, Switzerland*
[3]*Current address: deepXscan GmbH, Zeppelinstr. 1, D-01324 Dresden, Germany*
[4]*Current address: VAT Group, Seelistr. 1, CH-9469 Sennwald, Switzerland*
[*]*adam.kubec@psi.ch*

Abstract: The patterning of x-ray grating surfaces by electron-beam lithography offers large flexibility to realize complex optical functionalities. Here, we report on a proof-of-principle experiment to demonstrate the correction of slope errors of the substrates by modulating the local density of the grating lines. A surface error map of a test substrate was determined by optical metrology and served as the basis for an aligned exposure of a corrected grating pattern made by electron-beam lithography. The correction is done by a variation of the local line density in order to compensate for the local surface error. Measurements with synchrotron radiation and simulations in the soft X-ray range confirm that the effects of slope errors were strongly reduced over an extended wavelength range.

1. Introduction

Diffraction gratings are key components in experiments with UV, VUV and soft X-ray radiation at synchrotron radiation and free-electron laser (FEL) facilities. They are used in monochromators to produce beams with narrow energy bandwidth and in analyzers to provide high resolution spectral analyses of scattered radiation. Today, such diffraction gratings consist of a large number of periodic grooves (typically tens to thousands per millimeter) arranged on the reflecting surface of a plane or concave grating substrate. The spectral resolution of such gratings is of particular importance in soft Resonant Inelastic X-ray Scattering (RIXS) techniques as both, the monochromator in the incoming beam as well as the analyzer collecting the scattered radiation, limit the energy resolution of the setup. The resolving power of RIXS spectrometers is usually given as the ratio between photon energy E and the energy resolution δE. Values of E/δE > 10'000 are achieved in the soft X-ray range, and state of the art setups aim towards resolving powers of 100'000 [1]. This poses extremely stringent demands on the optical quality of the gratings used in the monochromator and the RIXS spectrometer.

The energy resolution of gratings is often affected by local slope errors of the grating substrates. For ultimate spectral resolution, the substrates need to be ultra-precise and superpolished, with shape errors of a few nanometers on a length of typically 100–300 mm, slope errors well below 100 nrad, and a roughness on the single digit angstrom range. Substrates with such specifications need to be produced according to complicated and expensive procedures including metrology steps and deterministic figuring techniques such as ion-beam figuring [2], elastic emission machining [3] or differential deposition [4]. However, even super polished Si-substrates made by elastic emission machining show periodic residual figure deviation in the range of few nanometers

[5] The line patterns of X-ray gratings are mostly produced either by holographic exposures of interfering laser beams into a photo resist [6,7], or by ruling machines that mechanically imprint the grating groves in a line-by-line manner into a metal layer [8]. Although these methods have shown good results for gratings with equidistant grating lines or a slow, continuous variation of the grating pitch (variable line spacing - VLS - gratings), they show little flexibility regarding the line patterns they can produce.

As an alternative to these established methods, a fabrication of the grating by electron-beam lithography (EBL) has the advantage that it allows for exposure of arbitrary line patterns with high resolution. Reflective-diffractive X-ray optics with complex functionality have been manufactured by EBL, e.g., combining energy dispersive and focusing properties [9]. The technique has continuously improved regarding speed and placement accuracy, making it suitable for the exposure of high quality diffractive X-ray patterns over large areas [10]. Detailed studies on EBL written reflective gratings for applications in X-ray astronomy have revealed that groove displacements of few tens of nanometers can be obtained even over large distances [11]. Moreover, the flexibility of EBL opens the possibility to produce diffractive elements that can be used to compensate errors of X-ray optical elements. Probst et al. have recently proposed an elegant concept of a diffractive corrector for XUV and soft X-ray wavefronts that are distorted by imperfections of X-ray mirrors [12]. However, no measurements proving the validity of this concept have been presented to date.

In this article, we experimentally demonstrate a related but conceptually simpler approach to compensate the effects of slope errors on the performance of X-ray reflection gratings. The flexibility provided by EBL allows us to modulate the local grating pitch such, that the induced change in diffraction angle corrects for the unwanted deflection caused by the slope errors. For this first proof-of-concept, we consider the simplest case of a planar reflection grating with a constant nominal line density. As reflection gratings for the X-ray regime are used at shallow angles, we write the relevant relation describing diffraction of a reflective grating as

$$m\lambda g = \cos\alpha - \cos\beta \tag{1}$$

where m denotes the diffraction order, λ the wavelength and g the line density. α and β are the incidence and diffracted exiting angle with respect to the surface (see Fig. 1) and we define both angles with a positive sign.
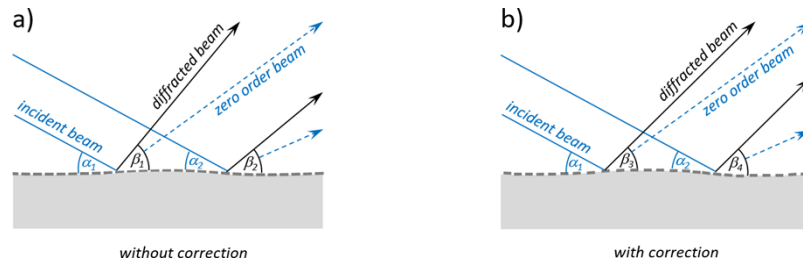
Fig. 1. Illustration of diffraction from a laminar grating on a deformed substrate. a) Uncorrected grating with constant line density, resulting in a variation of the first order deflection angles ($\alpha_1+\beta_1 \neq \alpha_2+\beta_2$). b) Corrected grating where the local line density of the grating is modulated such that the deflection angles are constant along the grating and the diffracted beams deflect in the same direction ($\alpha_1+\beta_3 = \alpha_2+\beta_4$).

As indicated in Fig. 1(a)), a substrate with slope errors will result in a variation of the local incidence angle α even for parallel incoming beams. For a constant line density g, the diffracted X-rays will have different deflection angles $\alpha+\beta$. To compensate for this effect, the local line density must be modulated such that the deflection angles are constant along the grating (see

Fig. 1(b)). If we describe the deformation of the substrate along the direction x by a modulation of the incidence angle by a local slope error $\delta(x)$, (1) is modified to yield the local line density for a corrected grating

$$g(x) = (m\lambda)^{-1}(\cos(\alpha_0 + \delta(x)) - \cos(\beta_0 - \delta(x))) \qquad (2)$$

where α_0, β_0 and g_0 are the nominal angles and line density in case of zero slope error, and $g(x) = g_0 + \Delta g(x)$ is the modulated line density to keep a constant deflection angle.

2. Preparation of slope error corrected X-ray gratings

In order to show a successful compensation of substrate deformations by measurements using synchrotron radiation, we produced a demonstrator grating for the soft X-ray range. The grating substrates were prepared to have significant deviations from a planar substrate. The errors are characterized by optical measurements. This provides the base for calculating the required pitch variation to compensate for the slope errors. An overview of the fabrication process is depicted in Fig. 2.
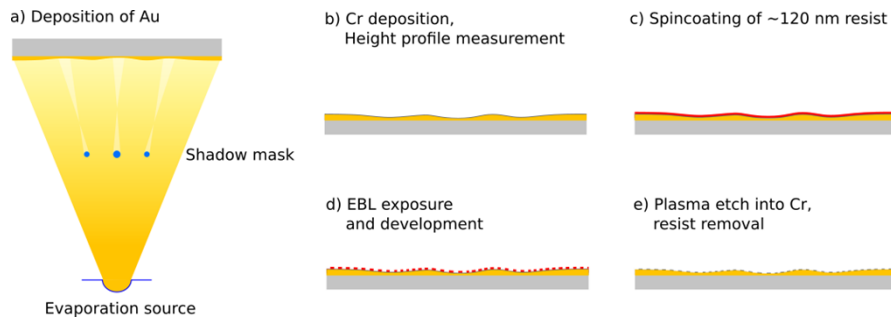
Fig. 2. Preparation of the test grating. a) The planar substrate is coated with Au by thermal evaporation through a shadow mask consisting of three rods, resulting in a thickness profile. b) deposition of 5 nm Cr and surface metrology, c) spincoating with resist, d) exposure of the grating by EBL and development of the resist, e) transfer of the grating structures into the Cr layer by plasma etching and removal of the resist.

2.1. Design of the demonstrator gratings

The gratings were designed for a photon energy of $E = 1$ keV (wavelength $\lambda = 1.2398$ nm). As the incidence and diffraction angles are shallow in the X-ray range, it is useful to define them with respect to the surface plane. We chose the nominal incidence angle and the diffraction angle to be $\alpha_0 = 1.43°$ (~25 mrad) and $\beta_0 = 1.72°$ (~30 mrad), respectively, to match the geometry of the setup for the synchrotron measurements as described further below. This results in a nominal line density $g_0 = 112.36$ mm^{-1} (grating pitch $p_0 = 8.9$ μm) according to (1), and a constant grating focusing factor $C_{ff} = sin\ \beta_0/sin\ \alpha_0 = 1.2$. The optimum step height h to maximize the diffraction efficiency of such a laminar reflection grating is $h = 11$ nm [13].

2.2. Preparation of the substrates

As substrates, we used commercially available 127 mm × 127 mm quartz photomask blanks with a thickness of 4.57 mm (Hoya Inc.). This thickness is about ten times smaller compared to typical grating substrates of the same lateral dimensions. However, they served their purpose as substrates for a demonstrator grating and can be readily loaded into the EBL tool. The substrate showed slope errors on the order of 1 μrad. In order to obtain grating substrates with significantly larger slope errors for demonstration of our method, an additional layer of Au was evaporated

onto the substrate. By applying a shadow mask about half way between the evaporation source and the substrate surface, the deposited thickness varied between approximately 300 nm and 900 nm (see Fig. 2(a)). On top of the Au layer, a ~5 nm thick layer of Cr was deposited, which later defined the step height of the resulting laminar grating. A step height significantly lower than the value required for optimum efficiency was chosen in order to assure that significant zero order efficiency is provided during the synchrotron measurements.

2.3. Optical metrology and data preparation

The height maps of the Au-coated substrate was measured with a Fizeau interferometer (Zygo Verifire) across a field of view of 100 mm diameter, recorded with a detector having 1000 × 1000 pixels. In order to minimize changes of the substrate shape, the same three point mount was used in the interferometer measurements and in the synchrotron experiments later on. The resulting interferometer data are shown in Fig. 3(a). The three dark vertical lines are caused by the penumbra of the shadow mask used during the Au evaporation process. A designated area for the grating was selected perpendicular to these lines, and a height profile was extracted, see Fig. 3(b), to yield the slope error profile by derivation, see Fig. 3(c). The slope error amounts to ~±40 μrad.
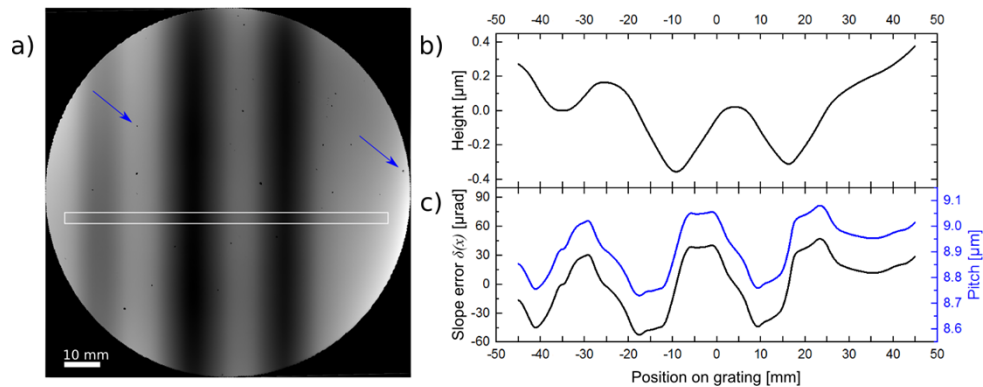
Fig. 3. a) Height map of a grating substrate after deposition of Au obtained from the Fizeau interferometer. The three dark vertical stripes represent the areas with reduced Au thickness caused by the penumbra of the shadow mask. The dark spots on the surface are caused by Au droplets deposited during the evaporation; two of which have been highlighted by blue arrows. The white rectangle represents the area of where the corrected grating was written (90 mm by 3 mm). b) Height profile along the highlighted box in the height map and c) the corresponding slope error $\delta(x)$ obtained by derivation of the height profile. The blue curve represents the local grating pitch for compensation of the slope errors calculated from Eq. (2) at 1 keV photon energy and an incidence angle of 1.43°.

The line profile from the interferometer data set was interpolated by a spline algorithm to give a smooth one-dimensional function along the designated grating area. This interpolation served as the input to calculate the required local value of the grating pitch Eq. (2) under the condition that the deflection angle is kept constant at $\alpha_0 + \beta_0 = 3.15°$ (~55 mrad), as shown by the blue curve in Fig. 3(c). This resulted in a list of grating line positions and widths of the corrected grating for the subsequent lithography step.

2.4. Grating fabrication by EBL

The substrates were spin coated with a 120 nm layer of poly-methyl methacrylate (PMMA) resist. Several gratings with a length of 90 mm and a width of 3 mm were exposed using the

Vistec EBPG5000plus EBL tool at the Paul Scherrer Institut. This also includes a grating with a constant pitch of 8.912 μm as a reference.

In order to cancel the effect of the local slope errors, a precise positioning of the exposed grating patterns with respect to the slope error map is required. This can be achieved by reference markers that are visible in the interferometer as well as in the EBL tool. In order to avoid a separate lithography step prior to the interferometer measurements to produce such markers, we used Au droplets that had been deposited unintentionally on the sample surface during the Au evaporation process. The alignment precision of this method was limited to ∼100 μm by the lateral resolution of the interferometer.

The exposure of the gratings was performed at a dose of 360 μC/cm^2 using a 100 nA beam at 100 kV acceleration voltage. The digital increment of the pattern generator for the placement accuracy of each individual line was set to an increment of 1 nm. The write field size of the EBL system covered by the magnetic electron beam deflection system was limited to 450 μm × 450 μm, so that the grating exposures consisted of many write fields stitched together using the laser interferometer controlled sample stage of the EBL system. In order to reduce effects of stitching errors or write field distortions, the grating patterns were exposed four times with offset stitching boundaries between the individual passes. The exposure of each grating took approximately 3 hours corresponding to a throughput of about 1 cm^2 per hour. After exposure the resist was developed in a 3:1 solution of isopropanol and methyl-isopropyl ketone (Fig. 2(d)), the pattern was transferred into the 5 nm thick Cr layer using a chlorine-based plasma, and the remaining resist was removed in an oxygen plasma (Fig. 2(e)).

3.   Synchrotron measurements

The experiments to characterize the corrected gratings were performed at the Surfaces/Interfaces Microscopy (SIM) beamline of the Swiss Light Source [14,15] at photon energies in the range of 800–1200 eV. Figure 4 shows a scheme of the setup. The photon energy is selected by a plane grating monochromator and focused onto a pinhole with 5 μm diameter to produce an intermediate source of radiation diverging towards the experimental chamber. 4.02 m downstream of this source, a 50 μm diameter aperture on a set of high precision translation stages selected a pencil beam to locally probe the grating. Closely downstream of the aperture, the substrate with the reflection gratings was placed on the same mount that was used for the characterization in the Fizeau interferometer (see section 2.3). The incidence angle was set to the nominal value of $\alpha_0 = 1.43°$ (∼25 mrad), resulting in a footprint of 50 μm × 2000 μm on the grating surface. At 3.56 m downstream of the center of the grating substrate a commercial in-vacuum Roper Scientific charge-coupled-device (CCD) camera with 1340 × 1300 pixels (h × v) with a pixel size of 20 μm × 20 μm was placed in the RESOXS [16] chamber at a vertical offset to collect both the zeroth and the first diffraction order of the grating. The pixel size of the detector corresponds to an angular increment of ∼5.6 μrad. The diffraction orders are separated by ∼5 mrad, corresponding to 17.8 mm (or 890 pixels) in vertical direction on the detector.

The aperture upstream of the grating is scanned in vertical direction in steps of 10 μm for a measurement. At each position of the aperture a different region along the inclined grating is illuminated. For an incidence angle of ∼25 mrad, an aperture scan of 2.4 mm is sufficient to cover the full 90 mm length of the gratings. The zeroth and first diffraction order beams are recorded by the CCD camera for each vertical position of the aperture. The vertical position of the beams on the detector is determined by integrating the camera signal in horizontal direction and fitting a one-dimensional Gaussian peak function. Using this approach the position of the beam can be determined with sub-pixel precision.

Figure 5(a) shows the resulting beam positions of the zeroth and the first diffracted order for an uncorrected and a corrected grating. For the uncorrected grating both orders show pronounced features caused by the slope errors of the substrate. Only the zeroth order is affected by the
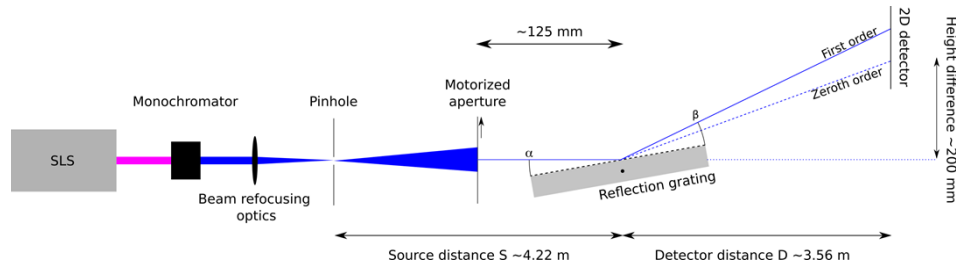
Fig. 4. Schematic side view of the experimental setup at the SIM beamline of the Swiss Light Source.

substrate errors for the corrected grating, whereas the first diffraction order produces a nearly linear trace on the detector.
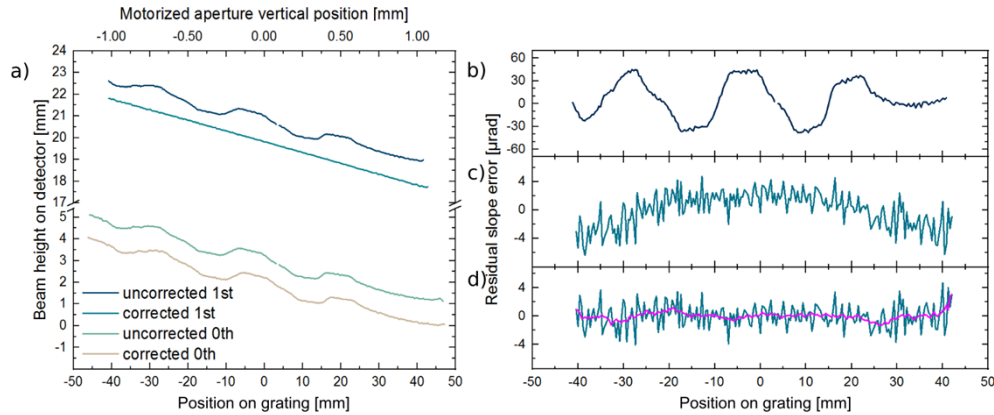
Fig. 5. a) Position of the zeroth and first diffraction orders of an uncorrected and a corrected grating on the detector as a function of the motorized aperture position. b) First order diffraction of an uncorrected grating and c) of a corrected grating after subtracting a linear fit. d) First order diffraction of the corrected diffraction grating after subtracting a quadratic fit. The magenta line shows the same data after smoothing by a 4 mm moving average filter.

4. Data analysis and discussion

In order to assess the quality of the slope error compensation of the corrected grating, we need to derive the uncompensated, residual slope error. It should be noted that the incidence angle of the pencil beam onto the grating surface changes for different positions of the motorized aperture, by about ±0.3 mrad for a vertical scan of ±1.2 mm due to the rather short distance from the secondary source. Moreover, the distance of the illuminated region of the grating to the detector changes during the pinhole scan. These effects can be corrected for by subtracting a linear fit from the curves of first diffraction order (top curves in Fig. 5(a)). The residual slope error is obtained by dividing the corrected positions on the detector by twice the detector distance. The resulting slope error curves are shown in Fig. 5(b) and (c). The graph for the uncorrected grating closely resembles the residual slope error curve shown in Fig. 3(c).

The curve for the corrected grating in Fig. 5(c), shows a clearly reduced residual slope error. However, the curve exhibits a parabolic shape, which can be explained by the fact that the change of incidence angle induces a slight change of the diffraction angle during the scan. To correct for

this well-known focusing effect of plane reflection gratings under divergent illumination [17], a quadratic fit is subtracted and the residuum is shown in Fig. 5(d). The curve shows residual slope errors of up to ±4 µrad on typical length scales of about 1 mm. The smoothened magenta curve in Fig. 5(d) reveals that the characteristic slope errors on centimeter length scales introduced by the shadow mask evaporation have disappeared. The remaining uncompensated residual slope error is below ±1 µrad.

Looking at Eq. (2) it is obvious, that the correction of substrate slope errors depends on the X-ray wavelength and thus on the photon energy. The question arises to what extent such a correction is successful for energies different from the design energy of 1 keV. Therefore, measurements for various energies between 800 eV and 1200 eV were performed. The incidence angle was kept constant at $\alpha_0 = 1.43°$ (~25 mrad). For the same setup simulations have been performed. The simulation was carried out assuming a point source at the pinhole location and the same geometric conditions as the experiment. The beam height on the detector was simulated as a function of the position on the grating. Then, the same analysis procedure was used on the simulation results to obtain Fig. 5(d) as described in Section 4.

The experiment and simulation results shown in Fig. 6 reveal, that the effectiveness of the correction is more and more reduced the further the photon energy deviates from the design energy. The same characteristic features observed for the uncorrected grating reappear. The sign of these features is opposite for energies above the design value of 1000 eV as compared to the shape of the surface, meaning that modulation of the grating line density is not sufficiently strong for a correction of the substrate slope errors, whereas for energies below the design energy, the slope errors are overcompensated. This is in agreement with Eq. (2), which shows that the required change in line density for a given slope error is proportional to the photon energy. However, the uncompensated residual slope errors are below ±10 µrad even for the extreme energies and therefore about four times smaller than the full slope errors observed in the diffraction from the uncorrected grating.
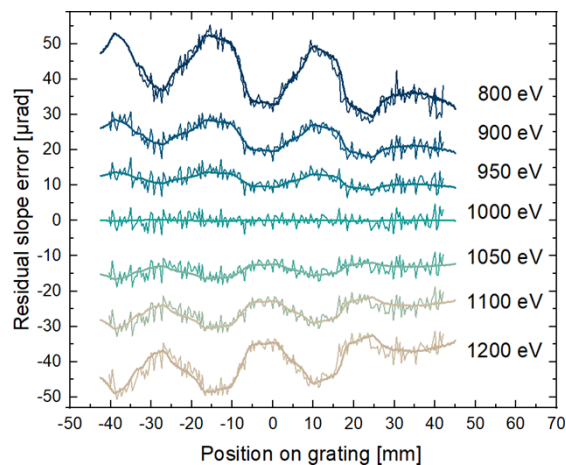
Fig. 6. Residual slope errors for measurements (jagged curves) and simulation (smooth curves) at various X-ray energies from 800 eV to 1200 eV. All curves were corrected with the same second order polynomial obtained by a fit to the data obtained at 1000 eV photon energy and vertically offset for clarity.

It is interesting to note that the high-frequency features of the measurements taken at different photon energies are not identical, however, they exhibit a high degree of correlation. The same type of partial correlation was found for measurements performed at the design energy on the

same grating, but with small offsets along the grating lines (not shown here). This indicates that these features are not caused by random errors in synchrotron measurements, but that they are indeed rooted in deformations of the substrate on millimeter length scales. As the optical metrology performed on the grating substrates was yielding height profiles, which had to be converted into slope errors by derivation, it is insensitive for detecting slope errors on short length scales. For example, the detection of a slope error of 1 μrad over a length of 1 mm would require detecting a height change of only 1 nm. This sensitivity is beyond the limits of the Fizeau interferometer used for the characterization of the substrates.

5. Simulations for other experimental conditions

The experiments used a fixed incident angle (α) for all the energies, whereas the deflection angle $\alpha + \beta$ was free ($\alpha + \beta \neq$ constant). Under the conditions that are commonly used for beamline monochromator, the deflection angle for each energy is the same (fixed-deflection angle geometry) or the incident and exit angle are both free (variable deflection angle geometry). In the fixed deflection angle geometry, $\alpha + \beta$ is constant for different energies. In the variable deflection angle geometry, $\alpha + \beta$ is not constant, and α is not fixed compared with the experimental case. Both geometries fulfil the condition for an ideal grating without slope error that the grating with a uniform line density, g satisfies the grating equation for different energies:

$$g = \frac{1}{\lambda_1}\{\cos(\alpha_1) - \cos(\beta_1)\} = \frac{1}{\lambda_2}\{\cos(\alpha_2) - \cos(\beta_2)\}. \tag{3}$$

Under the small-angle approximation, Eq. (3) gives

$$\frac{1}{\lambda_1}(\beta_1 + \alpha_1)[\beta_1 - \alpha_1] = \frac{1}{\lambda_2}(\beta_2 + \alpha_2)[\beta_2 - \alpha_2]. \tag{4}$$

The fixed-deflection angle solution is given by

$$\frac{1}{\lambda_2}(\beta_2 - \alpha_2) = \frac{1}{\lambda_1}(\beta_1 - \alpha_1), \tag{5}$$

$$\beta_2 + \alpha_2 = \beta_1 + \alpha_1 \tag{6}$$

while the variable deflection angle solution is

$$\frac{1}{\lambda_2}(\beta_2 + \alpha_2) = \frac{1}{\lambda_1}(\beta_1 + \alpha_1) \tag{7}$$

$$\beta_2 - \alpha_2 = \beta_1 - \alpha_1 \tag{8}$$

The fixed-deflection angle and variable deflection angle simulations were carried out using the same experimental geometry, only varying the values for α and β in a way that they satisfy the fixed-deflection angle and variable deflection angle conditions, respectively. The simulation results are shown in Fig. 7. The fixed-deflection angle condition is more commonly used for monochromators due to its simple geometry. On the other hand, the variable deflection angle condition is less sensitive to slope errors on the gratings when operating at different energies. The results from the simulations show that the method used in this paper for the correction can be effective also for energies that deviate from the design energy of the slope error correction; this is especially the case when using the variable deflection angle geometry.
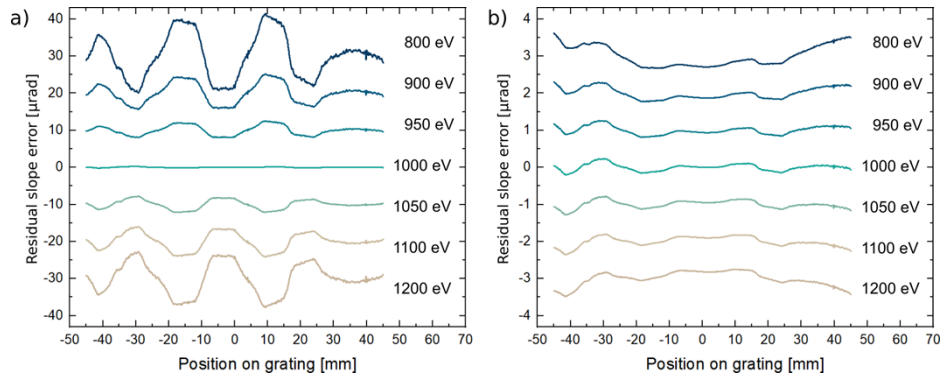
Fig. 7. simulation results for fixed-deflection angle (a) and variable deflection angle (b) geometry. Same as in Fig. 6, all curves were corrected with the second-order polynomial obtained by a fit to the data obtained at 1000 eV photon energy and vertically offset for clarity. In addition, the best linear fit was removed for each energy separately to clearly show the apparent residual slope error.

6.   Conclusions and outlook

We have designed and manufactured a demonstrator reflection grating for soft X-rays by means of EBL. The line density of the grating was varied along the grating such that the deflection angle of the first order diffracted beam would be constant and thereby compensates for slope errors of the grating substrate. The measurements performed with synchrotron radiation confirm that the effect of the substrate slope errors of approximately ±40 µrad could be reduced by approximately one order of magnitude. This proof-of-principle experiment demonstrates the feasibility of slope error compensation even though it was carried out on a grating with a rather low line density of ~100 lines per millimeter and on a low-quality substrate with very pronounced slope errors. The compensation effect is optimal at the design energy, however, investigations at varying energies indicate that the uncompensated residual slope errors are still significantly smaller than for an uncorrected grating. In addition, simulations show that compensations for the slope error is effective for different experimental conditions, such as, fixed-deflection angle and variable deflection angle geometries.

In the presented experiments, the results were limited by the accuracy of the optical surface measurement technique, especially regarding the slope error detection on short length scales. By applying more advanced metrology tools, we expect this approach to be capable of reducing the effects of grating substrate slope errors even further. Moreover, the method could be readily extended to the correction of two dimensional slope error maps. In this case the grating would consist of curved instead of straight lines.

The placement accuracy of modern EBL tools is on the order of a few tens of nanometers even over large patterns [10]. This corresponds to about 1/10 to 1/100 of typical pitches used in X-ray reflection gratings, thereby introducing corresponding wave front aberrations of λ/10 to λ/100. We therefore expect that the accuracy of the lithography will not limit the performance of the method. However, it should be noted that EBL tools are typically optimized for applications in micro-electronics and optoelectronics, and are therefore limited regarding the substrate sizes, thicknesses and surface curvatures that can be handled. This may require the development of customized EBL tools optimized for X-ray grating fabrication.

The presented method is an example for the inherent flexibility of EBL for X-ray grating fabrication. Once the metrology data are available, a slope error correction using the presented approach is straight-forward and takes little effort, as it essentially only requires a modification of

the exposure data files. This approach can therefore avoid costly steps for the removal of substrate slope errors by deterministic figuring techniques.

The key advantage, however, lays in the versatility of the EBL-based approach, which allows for the realization of X-ray optical designs with much higher degree of complexity as compared to gratings produced by ruling or holography. It is, for instance, quite natural in EBL to generate multiple patterns next to each other. This can be multiple gratings with different line densities, focusing properties (related to reflective zone plates) that would allow to omit an extra focusing mirror, or beam splitter gratings that would allow to send two copies of the beam to the experiment, for instance to do pump/probe experiments on the micro- to nanosecond time domain. Provided that metrology techniques with sufficient accuracy are available, it could possibly lead to X-ray reflection optics with specifications beyond what is possible today.

Disclosures. Adam Kubec is currently employed at XRnanotech GmbH, which can manufacture the structures presented in this work.

Data availability. Data underlying the results presented in this paper are not publicly available at this time but may be obtained from the authors upon reasonable request.

References

1. J. Dvorak, I. Jarrige, V. Bisogni, S. Coburn, and W. Leonhardt, "Towards 10 meV resolution: The design of an ultrahigh resolution soft X-ray RIXS spectrometer," Rev. Sci. Instrum. **87**(11), 115109 (2016).
2. M. Weiser, "Ion beam figuring for lithography optics," Nucl. Instrum. Methods Phys. Res., Sect. B **267**(8-9), 1390–1393 (2009).
3. K. Yamauchi, H. Mimura, K. Inagaki, and Y. Mori, "Figuring with subnanometer-level accuracy by numerically controlled elastic emission machining," Rev. Sci. Instrum. **73**(11), 4028–4033 (2002).
4. C. Morawe, S. Labouré, J.-C. Peffen, F. Perrin, A. Vivo, and R. Barrett, "X-ray mirror figure correction by differential deposition and off-line metrology," J. Synchrotron Radiat. **26**(6), 1872–1878 (2019).
5. F. Siewert, J. Buchheim, G. Gwalt, R. Bean, and A. P. Mancuso, "On the characterization of a 1 m long, ultra-precise KB-focusing mirror pair for European XFEL by means of slope measuring deflectometry," Rev. Sci. Instrum. **90**(2), 021713 (2019).
6. G. Schmahl and D. Rudolph, "High precision gratings produced holographically by means of reconstructed identical wave fronts," Optik **30**(6), 606–609 (1970).
7. S. Lemke, T. Seliger, I. Rudolph, O. Kutz, P. Goettert, B. Nelles, F. Senf, and B. Loechel, "Status of laminar grating manufacturing via lithography at HZB," Microsyst. Technol. **20**(10-11), 2061–2064 (2014).
8. F. Siewert, B. Löchel, J. Buchheim, F. Eggenstein, A. Firsov, G. Gwalt, O. Kutz, S. Lemke, B. Nelles, I. Rudolph, F. Schäfers, T. Seliger, F. Senf, A. Sokolov, C. Waberski, J. Wolf, T. Zeschke, I. Zizak, R. Follath, T. Arnold, F. Frost, F. Pietag, and A. Erko, "Gratings for synchrotron and FEL beamlines: a project for the manufacture of ultra-precise gratings at Helmholtz Zentrum Berlin," J. Synchrotron Radiat. **25**(1), 91–99 (2018).
9. T. Wilhein, D. Hambach, D. Niemann, M. Berglund, L. Rymell, and H. M. Hertz, "Off-axis reflection zone plate for quantitative soft x-ray source characterization," Appl. Phys. Lett. **71**(2), 190–192 (1997).
10. D. Lin, Z. Liu, K. Dietrich, A. Sokolov, M. G. Sertsu, H. Zhou, T. Huo, S. Kroker, H. Chen, K. Qiu, X. Xu, F. Schäfers, Y. Liu, E.-B. Kley, and Y. Hong, "Soft X-ray varied-line-spacing gratings fabricated by near-field holography using an electron beam lithography-written phase mask," J. Synchrotron Radiat. **26**(1), 1–10 (2019).
11. C. T. DeRoo, J. Termini, F. Grisé, R. L. McEntaffer, B. D. Donovan, and C. Eichfeld, "Limiting spectral resolution of a reflection grating made via electron-beam lithography," ApJ **904**(2), 142 (2020).
12. J. Probst, C. Braig, E. Langlotz, I. Rahneberg, M. Kühnel, T. Zeschke, F. Siewert, T. Krist, and A. Erko, "Conception of diffractive wavefront correction for XUV and soft x-ray spectroscopy," Appl. Opt. **59**(8), 2580–2590 (2020).
13. A. Franks, K. Lindsay, J. M. Bennett, R. J. Speer, D. Turner, and D. J. Hunt, "The theory, manufacture, structure and performance of NPL X-ray gratings," Phil. Trans. Roy. Soc. **277**, 503–543 (1975).
14. U. Flechsig, F. Nolting, A. Fraile Rodríguez, J. Krempaský, C. Quitmann, T. Schmidt, S. Spielmann, and D. Zimoch, "Performance measurements at the SLS SIM beamline," AIP Conf. Proc. **1234**, 319–322 (2010).

15. J. Krempaský, U. Flechsig, T. Korhonen, D. Zimoch, C. Quitmann, and F. Nolting, "Synchronized monochromator and insertion device energy scans at SLS," AIP Conf. Proc. **1234**, 705–708 (2010).
16. U. Staub, V. Scagnoli, Y. Bodenthin, M. García-Fernández, R. Wetter, A. M. Mulders, H. Grimmer, and M. Horisberger, "Polarization analysis in soft X-ray diffraction to study magnetic and orbital ordering," J. Synchrotron Radiat. **15**(5), 469–476 (2008).
17. H. Petersen, C. Jung, C. Hellwig, W. B. Peatman, and W. Gudat, "Review of plane grating focusing for soft x-ray monochromators," Rev. Sci. Instrum. **66**(1), 1–14 (1995).